Magnetic field forming Using Planar Multicoil Antenna to Generate Orthogonal H-Field Components

Ashwani Sharma, Ghanshyam Singh, *Senior Member, IEEE*, Deepak Bhatnagar, *Senior Member, IEEE*, Ignacio J. Garcia Zuazola, *Senior Member, IEEE*, and Asier Perallos

***Abstract*— Magnetic-field (H-Field) forming using planar multicoil transmitter antenna is presented. To address angular misalignment in inductive coupling systems, three orthogonal H-field components are formed in near-field zone of the transmitter antenna. This proposed magnetic field forming is performed by analyzing near-field distributions of various combinations of spatially distributed coils. The analytical study evolves into the planar multicoil design achieving three orthogonal components of H-field formed in target receiver area. The proposed antenna is realized in printed circuit board technology, simulated, and measured to validate the claim. The results corroborated with the analytical results and proved potential of the proposed design suitable for inductive coupling based applications like radio frequency identification, wireless charging, near-field communication, and medical implantation.**

***Index Terms*— Magnetic field forming, near-field antenna, planar coil antenna, wireless power transfer (WPT).**

I. Introduction

THE need of advanced technology for wireless power transfer (WPT) in applications like healthcare (e.g., medical implants and mobile consumables), real-time logistics (e.g., track-and-trace), radio frequency identification (RFID), wireless battery charging of mobile devices, and near-field communication (NFC) has attracted considerable attention recently. The technology widely used to wirelessly transfer power and information between Transmitter (Tx) and Receiver (Rx) is known as inductive near-field coupling. For instance, the RFID system employs inductive coupling between Reader (Tx) and Tag (Rx) systems [1] tunned to a wisely chosen common frequency of operation. For certain applications demanding relatively low data rate (106 kbps [2]) and a small read range ($<$ 1 m), the HF 13.56 MHz band is the preferred choice [3], [4] in very dense surroundings and is allocated worldwide for unlicensed use.

For an efficient inductive coupling, coil antennas are widely adopted at the Tx and the Rx sides [5]–[8], where the coils are parallelized (for instance, the coil planes are parallel with xy-plane) and having collinear axes (z-axis). In such arrangement, only perpendicular H-field component (H_z) originating from the Tx coil can contribute to the induced voltage V_{ind} in the Rx coil and hence maximized. For instance, in HF-RFID application, the geometry and the dimension of the reader coil are optimized to obtain a maximum H_z at a predefined tag location/read range [3], [7], [8]. A further H_z enhancement is achieved by utilizing multiturn coils at the Tx side [5], [7]–[9]. To remotely power implanted medical devices used for telemonitoring at 13.56 MHz, a system was developed in [10] using a single-turn coil Tx antenna of dimension 25 cm to produce robust H_z powering a six-turn coil Rx antenna of dimension 5 cm. Whereas, in [11], an implant Rx coil at a target distance of 3 cm was powered by an external spiral coil Tx antenna of dimension 8 cm. In [12], an external spiral 3-D Tx antenna was used to power batteryless biomedical implant consisting of sensors/actuators on laboratory animals for diagnosis and therapy applications. Whereas, in [13], an ingestible capsule consisting of Rx coil was powered by a three-turn external spiral antenna placed out of the body. Although, these systems are designed by presuming a perfect alignment of the Rx coil with the Tx coil, in practice, it is not guaranteed due to misplacement of the Rx and motion of implanted bodies. For instance, in applications like tracking-tracing using RFID, wireless capsule endoscope, medical implants, and wireless charging of mobile devices where a free movement (lateral and angular) of the Rx system is necessary, misalignment of the Rx coil with respect to the Tx coil is very likely. As a result, these systems suffer with misalignment (lateral and angular) problem degrading power transfer performance.

To mitigate lateral misalignment problem, several solutions have been proposed in the literature. For instance, manual or mechanical realignment of Tx coil for smart arena applications was adopted in [14] and [15], whereas, spiral-coils [16], multicoils [17], [18], and coil-arrays [19]

Manuscript received August 25, 2016; revised March 18, 2017; accepted April 9, 2017. Date of publication April 17, 2017; date of current version May 31, 2017. *(Corresponding author: Ashwani Sharma.)*

A. Sharma is with the Department of Electronics and Communication Engineering, Jaypee University of Information Technology, Waknaghat 173234, India, and also with the Deusto Institute of Technology, University of Deusto, 48007 Bilbao, Spain (e-mail: ashwani.sharma@deusto.es).

G. Singh is with the Department of Electronics and Communication Engineering, Malaviya National Institute of Technology, 302017, Jaipur, India (e-mail: gsingh.ece@mnit.ac.in).

D. Bhatnagar is with the Department of Physics, University of Rajasthan, Jaipur 302004, India (e-mail: dbhatnagar2010@gmail.com).

I. J. Garcia Zuazola is with the School of Electronic, Electrical, and Systems Engineering, Loughborough University, Leicestershire LE11 3TU, U.K. (e-mail: i.j.garcia-zuazola@lboro.ac.uk).

A. Perallos is with the Deusto Institute of Technology - DeustoTech, University of Deusto, 48007 Bilbao, Spain (e-mail: perallos@deusto.es).

Color versions of one or more of the figures in this paper are available online at http://ieeexplore.ieee.org.

Digital Object Identifier 10.1109/TAP.2017.2695009

were proposed for wireless changing platforms. Although such schemes can compensate lateral misalignment of the Rx coils, the angular misalignment problem still persists.

The angular misalignment problem degrades power transfer because the tilted planar Rx coil is able to capture only a fraction of the H_Z generated by a planar Tx coil antenna [20]. To mitigate this, a 3-D Rx antenna solution was adopted using three spatially distributed orthogonal coils to capture H_Z effectively oblivious to its tilt in wireless endoscopy capsule [21], [22], where Helmholtz coil and solenoid were used as external Tx antennas. In contrast, for applications favoring 'planar' Rx antennas due to cost and size limitations, e.g., RFID tags, wirelessly charged mobiles, and medical implants, the 3-D Rx antenna solution is not practical. Moreover, since the three orthogonal coils in the 3-D Rx can capture all the three orthogonal H-field components, the potential of 3-D Rx coil antenna is underutilized. This motivates to adopt the other solution that redesigns the Tx coil antenna using magnetic field forming technique for producing transverse fields (H_x and H_y) in addition to the vertical field (H_z) to address the angular misalignment problem.

The magnetic field forming is performed by constructive and destructive interferences of various H-field components originating from multiple spatially distributed Tx coils; this has been used in various wireless powering applications. For instance, a Tx antenna consisting of two perpendicular spiral coils in 3-D was used in [23], which generates two perpendicular H-field components to address angular misalignment of the Rx coil. Whereas, a Tx antenna consisting of two Tx coils arranged in cross was presented in [24] to produce directed magnetic beam. Designs having cubical Tx structure using pairs of coils (Helmholtz and circular) distributed on the faces of the cube were presented for wireless endoscopy [25] and power transfer [26]. By choosing appropriate phase shifts of the transmitting coils, magnetic field focusing within the cubical area was achieved. Moreover, [27] presented a 3-D bowl-shaped Tx antenna for charging small electronic devices, e.g., hearing aids and wearables. This antenna consisting of spiral loops and conical-shaped helical loops co-axially distributed in 3-D to generate H-fields within the bowl volume. A strong H_Z was produced by the bowl antenna, however, the orthogonal lateral H-field components were weak along the bowl axis. Therefore, a Tx antenna producing robust transverse fields (H_x and H_y) along with traditional vertical field (H_z) in target Rx area is sought. Furthermore, a planar design of the Tx antenna is preferred for its simplicity, cost effectiveness, and reliability. In this paper, we propose a planar multicoil Tx antenna designed using magnetic field forming to produce three orthogonal H-field components in the target Rx area. The proposed Tx antenna provides opportunity to exploit full potential of existing 3-D Rx coil antennas and relaxes the planar Rx coil design by powering it in almost all orientations.

The Rx coils used in the literature had the dimension ranging from 1 to 4 cm. For instance, Rx coils of diameter 1–2 cm in [10]–[13], [15], [21], [22], [25], and [27], 3 cm in [10], [16], [20], and [23], and 4 cm in [10] and [17] were presented. In this paper, the target Rx area is assumed to confine within 4×4 cm^2 at a distance of 5 cm away from the Tx antenna as considered in [9], [12], [13], [20], and [26].

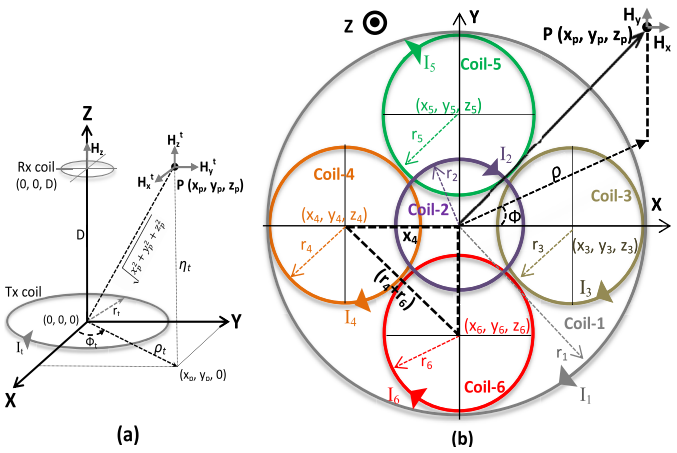

Fig. 1. (a) Inductively coupled Tx and Rx coils. (b) Planar multicoil Tx antenna.

This paper is organized as follows. Section II presents the proposed planar multicoil antenna modeling and design. The analytical evolution of the proposed design is described in Section III, which includes the field distribution analysis of spatially distributed coils composing the design. Section III-C demonstrates the field-distributions using analytical results. The final antenna realization is presented in Section IV and results are provided in Sections IV-A and V to validate the design. This paper is concluded in Section VI.

II. Planar Multicoil Antenna Design for Magnetic Field Forming

Inductive coupling systems wear loosely coupled coil antennas at the Tx and the Rx sides [Fig. 1(a)]. Represented in cartesian coordinate system, the Tx coil t, centered at location (x_t, y_t, z_t), which is same as the origin (0, 0, 0) in this figure, has radius r_t, a uniform total current amplitude I_t and phase θ_t, and the number of turns T_t each having current i_t, hence $I_t = T_t \times i_t$. An electrically small circular coil [28] antenna is considered such that the current I_t can be assumed uniform throughout the length of the wire; this forces the originating H-field components to add in phase and positively contribute to the near-field [8]. The oscillating H-field originating from the Tx coil induces power in the Rx coil situated at a distance D (read range) along z-axis. To analyze the H-field distribution around the Rx coil location, analytical modeling of H-fields originating from the Tx coil is required.

Considering H-field due to the Tx coil at an arbitrary observation point P (x_p, y_p, z_p), the relative distances and angle ρ, η, and ϕ defined in Fig. 1(a) can be calculated as

$$\begin{aligned} \rho_t &= \sqrt{(x_p - x_t)^2 + (y_p - y_t)^2} \\ \eta_t &= z_p - z_t \\ \phi_t &= \tan^{-1}\left[\frac{y_p - y_t}{x_p - x_t}\right]. \end{aligned} \tag{1}$$

The three orthogonal components H_x, H_y, and H_z of H-field at P shown in Fig. 1(a) are formulated in [20] and for free

space medium given by

$$H_\rho^t = \frac{I_t e^{j\theta_t}\eta_t}{2\pi\rho_t\sqrt{(r_t+\rho_t)^2+\eta_t{}^2}}\left[\frac{r_t^2+\rho_t{}^2+\eta_t{}^2}{(r_t-\rho_t)^2+\eta_t{}^2}E(\kappa)-K(\kappa)\right]$$
$$H_x^t = H_\rho^t\cdot\cos(\phi_t),\quad H_y^t = H_\rho^t\cdot\sin(\phi_t)$$
$$H_zt = \frac{I_t e^{j\theta_t}}{2\pi\sqrt{(r_t+\rho_t)^2+\eta_t{}^2}}\left[K(\kappa)+\frac{r_t^2-\rho_t{}^2-\eta_t{}^2}{(r_t-\rho_t)^2+\eta_t{}^2}E(\kappa)\right] \tag{2}$$

where $\kappa = ((4r_t\rho_t/(r_t+\rho_t)^2+\eta_t{}^2))1/2$, and $K(\kappa)$ and $E(\kappa)$ are the complete elliptic integrals of the first and second kinds, respectively. Using (1) and (2), the three H-field components at any arbitrary observation point (x_p, y_p, z_p) in the near-field of a coil antenna centered at any arbitrary location (x_t, y_t, z_t) can be found; this is used next to analyze the fields.

Initially, we consider a planar single-coil Tx antenna centered at the origin (0, 0, 0) and a planar Rx coil (of size very small compared with the Tx coil) located on the z-axis at (0, 0, D) [Fig. 1(a)], and the H-field at the Rx location is calculated using (2) by substituting $\rho_t = 0$, $\eta_t = D$, and $\phi_t = 0$ to obtain

$$H_x = 0, H_y = 0,\quad H_z = \frac{I_t r_t^2}{2\left[\sqrt{(r_t^2+D^2)}\right]^3}. \tag{3}$$

The Tx coil is desired to produce robust H-field in the near-field zone, and therefore, the geometry (coil size r_t) of the Tx coil is optimized to obtain a maximum H-field for a given read range D. To maximize H-field at a predefined D, (3) is differentiated with respect to r_t and equated to zero. Since only H_z exists $(\partial/\partial r_t)(H_z) \implies 0)$, this results into an optimum r_t derived as a function of D as $r_t = (2D)1/2$ in [4] and [8]. Therefore, the maximum dimension of the Tx coil is limited by the read range D, which is also followed for the design proposed in this paper.

We note from (3) that along the axis of the Tx coil where $\rho_t = 0$, the H-field components (H_x and H_y) parallel to the Tx coil plane vanish. Since the planar Tx coil is lying in xy-plane, only the z-component (H_z) of H-field is dominantly produced along its axis. Therefore, for an effective power transfer, the Rx coil is desired to be parallel with xy-plane and aligned with the Tx coil to effectively capture H_z, as illustrated in Fig. 1(a). The angular misalignment between the two coils causes reduction in power transfer, because only a fraction of H_z originating from the Tx coil induces the Rx coil. To mitigate the angular misalignment problem, a 3-D Rx antenna can be accomplished using three orthogonal coils to ideally capture full H_z oblivious to the Rx rotation; however, planar Rx antennas are favored for certain applications due to simplicity and cost effectiveness. A novel design of the Tx antenna is required to produce nonzero lateral fields (H_x and H_y) along with traditional vertical field (H_z); this improves the power transfer in case of misalignment, leading to a relaxed Rx coil design. The proposed Tx coil antenna is presented in Section II-B and designed by magnetic field forming of three orthogonal H-field components, beneficial for both applications, the planar, and the 3-D Rx coil antennas.

TABLE I
DESIGN PARAMETERS OF PROPOSED MULTICOIL ANTENNA

coil-i	x_i (cm)	y_i (cm)	z_i (cm)	r_i (cm)	I_i (A)	θ_i
coil-1	0	0	0	7.07	1	$\pi/2$
coil-2	0	0	0	2.50	2	$\pi/2$
coil-3	4.1	0	0.08	2.90	2	0
coil-4	-4.1	0	0.08	2.90	2	π
coil-5	0	4.1	0.08	2.90	2	0
coil-6	0	-4.1	0.08	2.90	2	π

A. Planar Multicoil Antenna Modeling

A planar multicoil antenna structure consisting of N planar coils is depicted in Fig. 1(b), where each coil-i, $\forall i \in [1, N]$, is parallel to xy-plane and centered at location (x_i, y_i, z_i), has radius r_i, a uniform total current amplitude I_i and phase θ_i, and number of turns T_i each having current i_i, hence, $I_i = T_i \times i_i$. At an arbitrary observation point P (x_p, y_p, z_p) shown in Fig. 1(b), the H-field originating from the multicoil antenna is analyzed, and the field components H_x^i, H_y^i, and H_z^i due to coil-i are calculated using (1) and (2) and used to evaluate total fields H_x, H_y, and H_z at P [Fig. 1(b)]; this is given by summation of individual field components contributed by each coil-i, $\forall i \in [1, N]$, at P as

$$H_x = \sum_{i=1}^{N} H_x^i;\quad H_y = \sum_{i=1}^{N} H_y^i;\quad H_z = \sum_{i=1}^{N} H_z^i. \tag{4}$$

As in Section II [Fig. 1(a)], we consider the planar multicoil Tx located at the origin (0, 0, 0) and the planar Rx coil located on the z-axis at (0, 0, D). In case of a single coil Tx antenna, we showed in (3) that H_x and H_y are zero and only H_z is dominantly produced at the Rx location. Therefore, we use a planar multicoil Tx antenna to improve H_x and H_y along with H_z. For this purpose, magnetic field forming is utilized to obtain robust orthogonal H-field components at the read range D by carefully selecting the following design parameters, x_i, y_i, z_i, r_i, I_i, θ_i, and $\forall i \in [1, N]$ of the multicoil antenna that is proposed next.

B. Proposed Multicoil Design for Magnetic field forming

In this section, the proposed multicoil antenna is designed to generate three orthogonal H-field components H_x, H_y, and H_z of (4) at a given read range $D = 5$ cm using magnetic field forming technique. The proposed design depicted in Fig. 1(b) is made of $N = 6$ coils, where coil-1 and coil-2 are concentric with the origin and lying in $z = 0$ plane. Coil-3, -4, -5, and -6 are inscribed within coil-1 and lying in $z = 0.8$ mm plane to avoid metallic short circuiting with coil-2. Without loss of generality, we assume a normalized current in each coil with respect to coil-1 implying $I_1 = 1$. The corresponding values of the parameters of the proposed design are listed in Table I. How the magnetic-field is analytically formed in the evolution of the final design is analytically demonstrated in Section III.

III. EVOLUTION OF THE PROPOSED DESIGN AND ANALYTICAL RESULTS

In this section, we present analytical evaluation of various parameters of the proposed multicoil antenna that consisted of

six coils where coil-1 and coil-2 were responsible for a robust H_z forming, whereas, coil-3, -4, -5, and -6 were designed to form H_x and H_y simultaneously in the target Rx area. The dimension of the Rx coil at $z = D = 5$ cm was assumed to confine within the range $-2 \leq x \leq 2$, $-2 \leq y \leq 2$ in cm, and hence, robust H_x, H_y, and H_z were formed within this area.

A. Analyzing Near-Fields of the Individual Coils −1 to −6

Initiating with the coil-1 which essentially resembles with a single-coil antenna centered at the origin, the paragraph immediately followed by (3) in Section II dictates optimal coil radius $r_1 = (2_1/2)D = 7.07$ cm to maximize H_z at $D = 5$ cm. Therefore, the maximum dimension of the proposed design is restricted to $2r_1 = 14.14$ cm. The normalized current in coil-1 was defined as $I_1 = 1$ A. The resulting H-field distributions in $z = D$ plane due to coil-1 are calculated using (2) and plotted (aided by MATLAB) in Fig. 2(a).

The H_x^1 and H_y^1 vanish in the target Rx area $-2 \leq x \leq 2$; $-2 \leq y \leq 2$, whereas, the H_z^1 magnitude is almost uniform within this range. However, there exist some areas where H_x^1 and H_y^1 are effective but their maximums occur far away (~ 7 cm) from the target Rx location ($x = y = 0$). The H-field distributions of coil-2 with radius $r_2 = 2.5$ cm are plotted in Fig. 2(b), where similar observations as the coils-1 can be drawn about H_x^2 and H_y^2, having a visible null, and H_z^2 having maxima at the target location $x = y = 0$. However, for coil-2, maximums of H_x^2 and H_y^2 are seen at ~ 3 cm and the H_z^2 field confinement is more focused. This shows that coil-1 and coil-2 contribute toward dominant H_z forming, whereas, H_x and H_y field-forming in the target Rx area is still required.

Considering coil-i $\forall i \in [3, 4, 5, 6]$ having parameters listed in Table I, corresponding H-field distributions in the Rx plane z $= D = 5$ cm are analyzed in Fig. 2(c)–(f). Essentially, the H-field patterns of coil-i are similar to that of coil-2; however, they are shifted versions corresponding to the spacial locations of coil-i with respect to coil-2. The following interesting observations are noted. For coil-3 and coil-4 in Fig. 2(c)–(d), the H_y^i and H_z^i are inferior near $x = y = 0$, however, the maximums of the H_x^i fall within the target Rx area and therefore can contribute positively toward the H_x field forming in the proposed design. Similarly, for coil-5 and -6 in Fig. 2(e)–(f), although H_x^i and H_z^i are inferior near $x = y = 0$, the maximums of the H_y^i dominate in the target Rx area and therefore can serve to the H_y field forming in the proposed design.

B. Combining Coil-1 to-6 for the Proposed Antenna Evolution

Following the discussion of Section III-A, coil-3, -4, -5, and -6 are used for H_x and H_y fields forming by combining them judiciously for a maximum field in the target Rx area. Due to symmetry, the coils have an equal current amplitude $I_3 = I_4 = I_5 = I_6$ (Table I). The current phases θ_i are chosen such that the individual H_x^is and H_y^is of four coils add constructively in the target Rx area. This results in $\theta_3 = \theta_5 = 0$ and $\theta_4 = \theta_6 = \pi$ as given in Table I. For a maximum field contribution of coil-3, -4, -5, and -6 toward H_x and H_y, the size of each coil is maximized by avoiding metallic shorting between the coils. Fig. 1(b) shows the final arrangement where the center location and radius of each of the four coils were found using geometrical calculations. This reveals $r_i = r_1/(1 + (21/2))$ $\forall i \in [3, 4, 5, 6]$; $x_3 = y_5 = (21/2)r_1/(1 + (21/2))$; and $x_4 = y_6 = -(21/2)r_1/(1 + (21/2))$, for rest of the coordinates $x_i = y_i = z_i = 0$ $\forall i \in [3, 4, 5, 6]$; the calculated values are provided in Table I. The field distribution of this joint design in Fig. 3(a) shows that robust H_x and H_y are obtained near $x = y = 0$ complementing one part of the final design, whereas, the H_z is not favorable at the target location. Since Section III-A revealed that coil-1 optimized H_z in the target Rx area but had nulls of H_x and H_y, the joint design containing coil-3, -4, -5, and -6 is combined with coil-1 for a joint H_x, H_y, and H_z field forming.

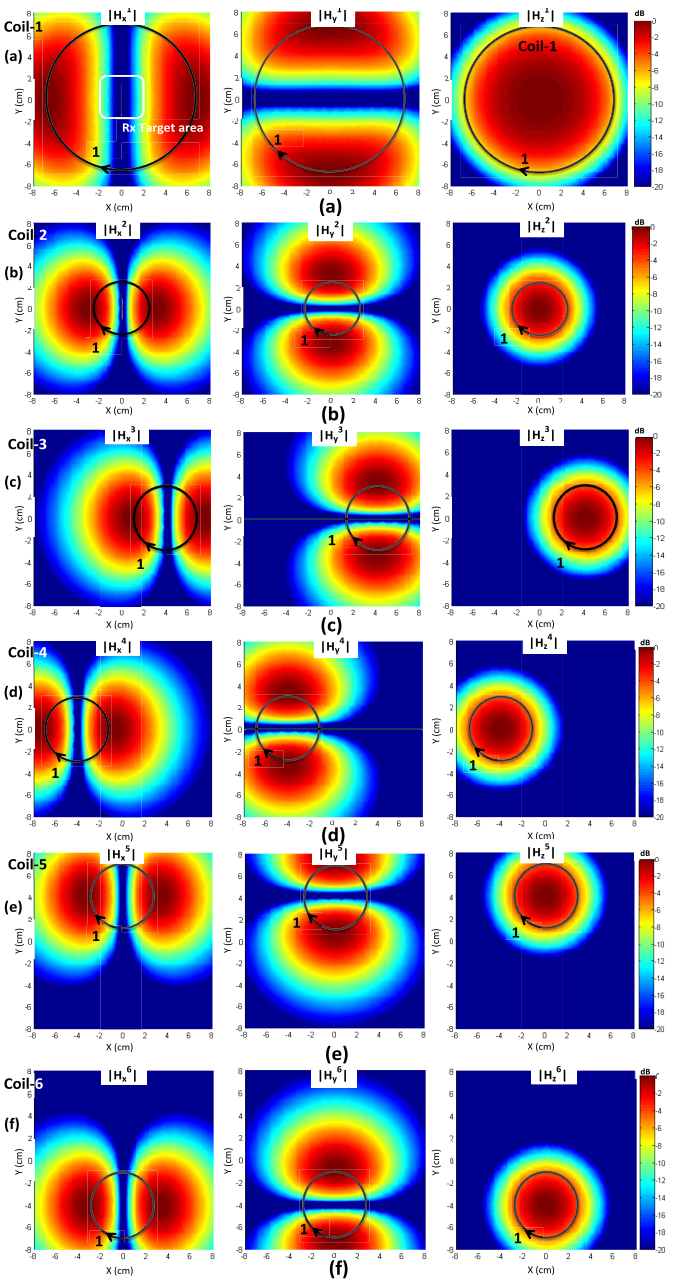

Fig. 2. Normalized analytical H-field distribution in $z = D = 5$ cm plane for (a) coil-1, (b) coil-2, (c) coil-3, (d) coil-4, (e) coil-5, and (f) coil-6.

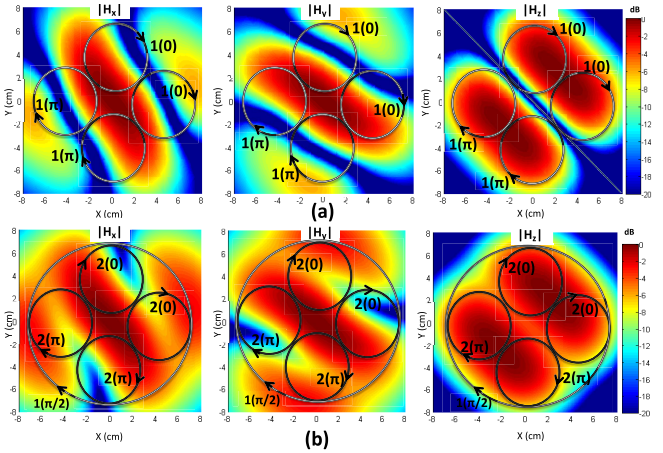

Fig. 3. Normalized analytical H-field distribution in $z = D = 5$ cm plane for (a) joint coil-3-4-5-6 and (b) joint coil-1-3-4-5-6.

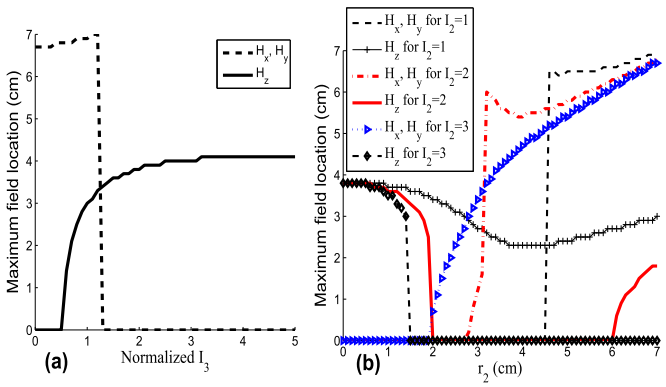

Fig. 4. Variation of maxima location of H-field components versus (a) I_3 and (b) r_2 and I_2.

The field distributions of a joint coil-1-3-4-5-6 are plotted in Fig. 3(b), which shows robust components H_x and H_y contributed by coil-3-4-5-6 and an improved H_z contributed by coil-1. Since the H_z is orthogonal to H_x and H_y, a solution of phase θ_1 that combines two orthogonal fields from coils-1 and 2 was found to be $\theta_1 = \pi/2$. A comparison of the field distributions of this joint venture presented in Fig. 3(b) with those of the original coil-1 of Fig. 2(a) reveals that the joint coil-3-4-5-6 design forces the maximums of H_x and H_y to fall near $x = y = 0$, while, drags the H_z maxima away from $x = y = 0$. Hence, the locations of maximum fields depend on coil-3-4-5-6 domination over coil-1 and is governed by normalized current amplitudes ($I_3 = I_4 = I_5 = I_6$) of the coils. To find suitable current amplitudes of coil-3-4-5-6 toward forming three orthogonal H-field components in the target Rx area, the effect of I_3 (hence I_4, I_5, and I_6) on maximum field location (distance of maxima from (0, 0, D)) was evaluated and the results demonstrating this were shown in Fig. 4(a). For $I_3 = 0$, which implies the design having only coil-1, the location of maximum of H_x and H_y is $\sim$ 7 cm and of H_z is zero, corroborating the observations made from Fig. 2(a). As I_3 increases, coil-3-4-5-6 starts dominating, hence, the H_x and H_y start dominating near $x = y = 0$ for $I_3 > 1.3$ and the H_z maxima moves away from $x = y = 0$ for $I_3 > 0.5$; choosing a higher I_3 is discouraged due to degradation in the H_z within target Rx area. Moreover, since I_3 is normalized with respect to I_1 ($I_1 = T_1 = i_1 = 1$), the integer values of I_3 are preferred because it becomes easier for practical realization of the coils by realizing normalized integer currents (e.g., I_3) into number of turns (e.g., $T_3 = I_3$, $i_3 = 1$). Therefore, the most suitable value for the normalized current was found from Fig. 4(a) to be $I_3 = 2$, which is the least possible integer for a finite H_x and H_y field forming in the target Rx area. For $I_3 = 2$ (hence, $I_4 = I_5 = I_6 = 2$), the maximums of H_x and H_y fall within the target Rx area, whereas the H_z maxima lies $\sim$ 3.8 cm away from $x = y = 0$; this can be observed from the field distribution plots of coil-1-3-4-5-6 in Fig. 3(b).

To bring the H_z maxima back to the desired location without affecting the favorable H_x and H_y distributions formed by coil-1-3-4-5-6, next, we judiciously add coil-2 to evolve into the final prototype [Fig. 1(b)]. Since coil-2 dominantly contributes toward forming the H_z maxima at $x = y = 0$ similar to coil-1, the center of coil-2 is located at (0, 0, 0) and the current phase is selected $\theta_2 = \pi/2$ to complement coil-1. The r_2 and I_2 of coil-2 was optimally found such that a robust H_z field forming close to $x = y = 0$ was achieved in the final design while maintaining the H_x and H_y maximums formed by coil-1-3-4-5-6 at $x = y = 0$. The effect of design parameters r_2 and I_2 of coil-2 on the maximum field locations of the final design (consisting coil-1 to -6) is shown in Fig. 4(b). For $r_2 \sim 0$, which essentially implies coil-1-3-4-5-6 design, the H_z maxima location is $\sim$ 3.8 cm and the maximums of H_x and Hy are situated at $x = y = 0$. As r_2 increases from zero, the H_z maxima moves toward $x = y = 0$ favoring the H_z field-forming. However, a high r_2 (limited by r_1) forces the H_x and H_y maximums beyond the desired location. Fig. 4(b) includes only integer values of I_2 due to simplification in practical design realization by converting integer current (I_2) into number of turns (T_2 for normalized $i_2 = 1$). It is observed from Fig. 4(b) that for $I_2 = 1$, r_2 has no solution to bring the H_z maxima back to $x = y = 0$. Whereas, for $I_2 = 2$ and $I_2 = 3$, ranges $2 \leq r_2 \leq 2.9$ and $1.5 \leq r_2 \leq 1.9$ respectively exist for which the H_z maxima moves back to $x = y = 0$ while keeping H_x and H_y maximums at $x = y = 0$. Since, currents are normalized with respect to the I_1, if $I_2 = 3$, therefore $1.5 \leq r_2 \leq 1.9$, then, coil-3 would lead to a higher number of turns in a small area of radius r_2 for certain applications and hence would be challenging to fabricate. Therefore, we judiciously choose $I_2 = 2$ as the favorable solution and $r_2 = 2.5$ cm as an approximate middle point of corresponding range $2 \leq r_2 \leq 2.9$ and coil-2 used for fine-tunning of the three orthogonal field components generated by the proposed multicoil antenna.

C. Analyzed Field Distribution Results of the Proposed Design

In this section, the H-field distributions of the final design evolved in Section III-B and drawn in Fig. 1(b) are analyzed. Using the design parameters listed in Table I, distributions of the components H_x, H_y, and H_z originating from the

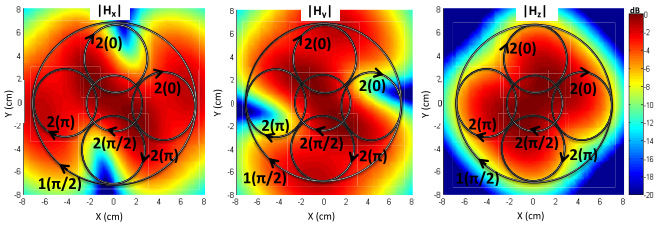

Fig. 5. Normalized analytical H-field distributions in $z = D = 5$ cm plane for the proposed planar multicoil antenna (coil-1-2-3-4-5-6).

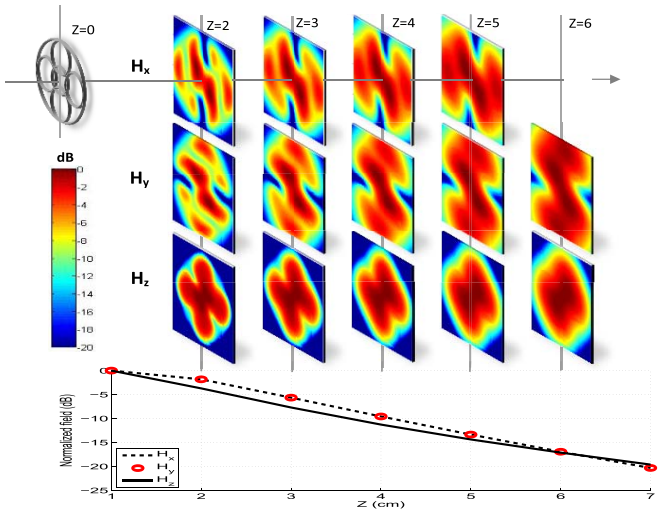

Fig. 6. Normalized analytical H-field distribution variation along the axis (z-axis) of the proposed multicoil antenna.

proposed planar multicoil antenna are calculated using (4) and plotted in Fig. 5 for the target Rx plane $z = D = 5$ cm. The analytical results show that robust H_x, H_y, and H_Z dominating in the target Rx area $-2 \leq x \leq 2$; $-2 \leq y \leq 2$ is achieved by the proposed design. The variation of the distribution of H-field components along the axis of the proposed antenna is presented in Fig. 6, where 2-D field-distributions show that, although the strength of the H-field reduces with distance, the targeted magnetic field forming is achieved for $z > 3$ cm. Hence, the results prove that the proposed antenna has the potential to magnetic field forming of three orthogonal vector components dominating in the target Rx area.

IV. Proposed Antenna Realization and Simulations

In this section, the analytically designed multicoil Tx antenna proposed in Section II-B is realized into a practical design and validated by simulation. The frequency of operation was 13.56 MHz chosen for compatibility with the HF-RFID applications. Since the proposed multicoil antenna presented in Fig. 1(b) with geometric parameters listed in Table I is a planar structure, printed circuit board (PCB) technology is chosen for its cost effective solution for this antenna realization. For this purpose, a two-sided FR4 substrate of thickness, $h = 0.8$ mm, relative dielectric constant $\epsilon_r = 4.4$, loss tangent $\tan\delta = 0.02$, and 0.02 mm of copper deposition was used. The realized structure is presented in Fig. 7 and

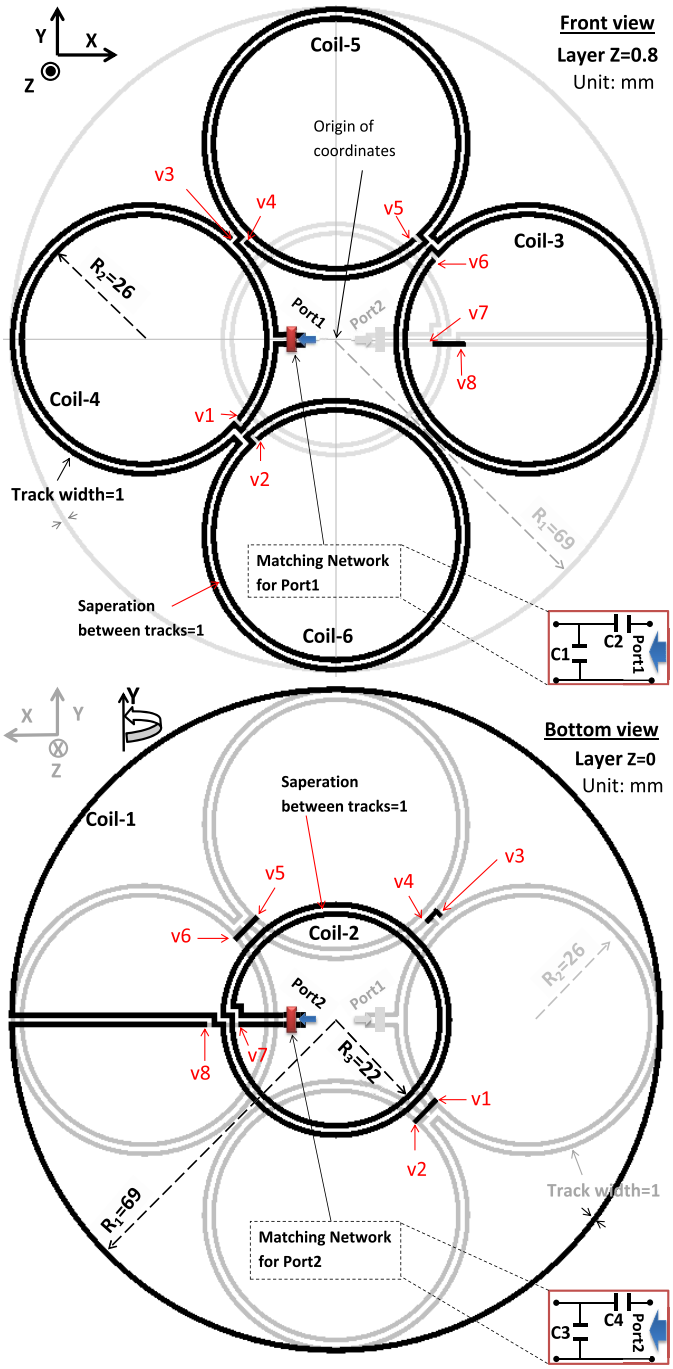

Fig. 7. Proposed planar multicoil antenna realization in PCB technology.

consisted of coil-3-4-5-6 etched on the front-side (layer $z = 0.8$ mm) and coil-1-2 on the bottom-side (layer $z = 0$) of the substrate and made of copper tracks of width $d = 1$ mm. The realized structure contained eight vias, v1-v8, to connect different parts of the coils etched on two sides of the substrate. Metallic continuity exists between two vias of following pairs, v1-v2 (bottom view), v3-v4 (bottom view), v5-v6 (bottom view), and v7-v8 (front view) as shown in Fig. 7.

The parameters of Table I are judiciously realized to comply with the practical antenna design. Typically, to feed each coil

with corresponding I_i and θ_i, a complex feed network is generally required. In this paper, the complex feed network is avoided by adopting the following arrangements; fed equal currents $i_i = 1$ A in each turn of all the coils and converted I_i values directly into N_i using $I_i = N_i \times i_i$, translated current phases $\theta_i = \pi$ of the coils into opposite circulations (e.g., counterclockwise) of their currents compared with the current circulations (clockwise) of the coils having $\theta_i = 0$. This resulted into one turn for coil-1 and two turns for each coil-2-3-4-5-6 with specific connectivity between turns (desired current circulations) as shown in Fig. 7. All the turns of coil-3-4-5-6 were connected in series and fed through a common Port1 with current amplitude 1 A and phase zero; the turns were wisely connected in a way that the currents in coil-3 and coil-5 flow opposite to the currents in coil-4 and coil-6, hence, the phase difference of π was simply realized by this geometrical arrangement. Since both coil-1 and coil-2 have current phases $\pi/2$ compared with the rest of the coils, they were connected in series so that the currents in both the coils have same anticlockwise circulation and fed through Port2 with current amplitude 1 A and phase $\pi/2$.

Hence, the realized structure (proposed antenna) is fed through Port1 and Port2 with two signals of equal amplitudes and $\pi/2$ phase difference; this simplifies significantly the feed network design if the coils 1 to 6 were individually fed. A power divider with $\pi/2$ phase (e.g., 90° hybrid) can be used to feed the 2-port structure. For maximum power delivery to the antenna at 13.56 MHz, impedances at Port1 and Port2 were matched to 50 Ω using L-section matching networks, each consisting of two capacitors, $C1$ and $C2$ at Port1, $C3$ and $C4$ at Port2, as shown in the insets of Fig. 7.

A. Simulation of the Proposed Antenna and Results

The proposed multicoil antenna design of Fig. 7 was simulated using Zeland IE3-D, based on the method of moments. Initially, the unloaded coil antenna was simulated to evaluate input impedances at the two ports (Port 1 and 2), and the requuired matching network parameters are calculated as $C1 = 26.131$ pF, $C2 = 35.142$ pF, $C3 = 73.279$ pF, and $C4 = 55.932$ pF. The matched antenna (with corresponding matching networks) was then simulated for validation. For fair comparison with the analytical results presented in Section III-C, each port fed with 1-A peak current and the results were normalized.

The S11 and S22 responses of the proposed multicoil antenna are shown in Fig. 8, which shows the antenna resonating around 13.56 MHz at both the ports and a ∼700 KHz (13.22–13.92 MHz) measured at −10 dB bandwidth. The S21 response is included in Fig. 8, which shows a negligibly small coupling between Port 1 and Port 2, and hence a good isolation between the two ports.

To validate the orthogonal magnetic field forming, the near-field distributions were simulated for a target Rx plane $z = D = 5$ cm. The simulated current flow indicated by vectors in each coil composing the multicoil antenna is shown in Fig. 9(a). Because of the electrically small size of the coils, a uniform co-phased current was observed along the tracks of each coil. The current circulations of coil-3-5 were

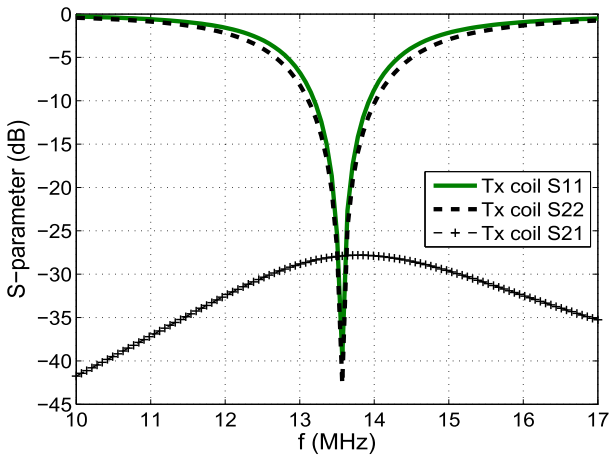

Fig. 8. S-parameter response of the proposed multicoil antenna.

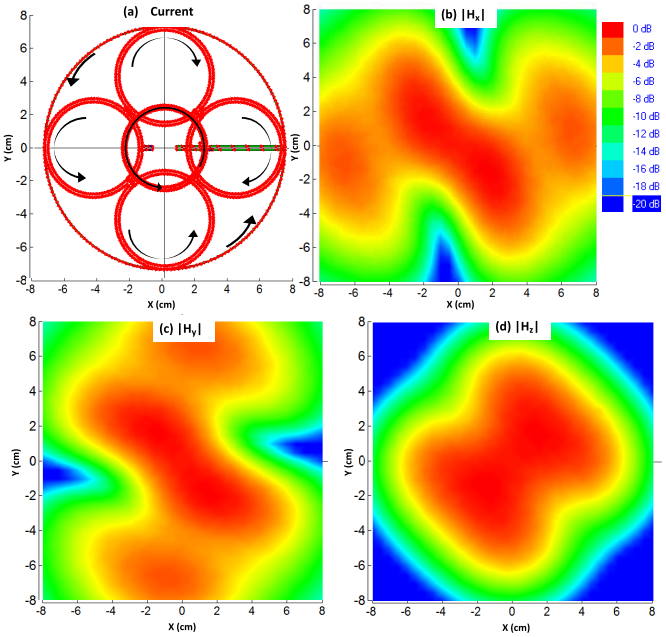

Fig. 9. Simulated multicoil antenna results. (a) Currents and (b)–(d) normalized H_x, H_y, and H_z distributions in $z = D = 5$ cm plane.

clockwise whereas that of coil-4-6 were counterclockwise (a phase difference of π); this corroborates the analytical current circulations presented in Fig. 5. The simulated currents of coil-1-2 were in-phase, circulated counterclockwise, and had a phase difference of $\pi/2$ with respect to coil-4-6. The simulated H_x, H_y, and H_z distributions of the proposed antenna in $z = 5$ cm plane are plotted in Fig. 9(b)–(d), respectively, which corroborate with those analytically obtained and presented in Fig. 5. The analytical and simulated H-field profiles are compared in Fig. 10 showing strong H_x, H_y, and H_z fields formed in the targeted region by the proposed antenna. The results validate the proposed antenna claim to generating three orthogonal components through magnetic field forming. The fabrication and measurements of the proposed antenna are presented subsequently.

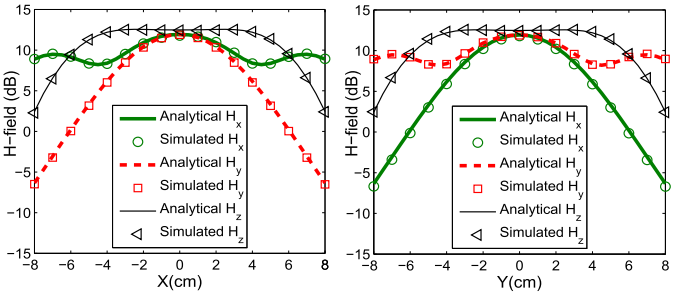

Fig. 10. H-field distributions of the proposed coil antenna at $z = 5$ cm.

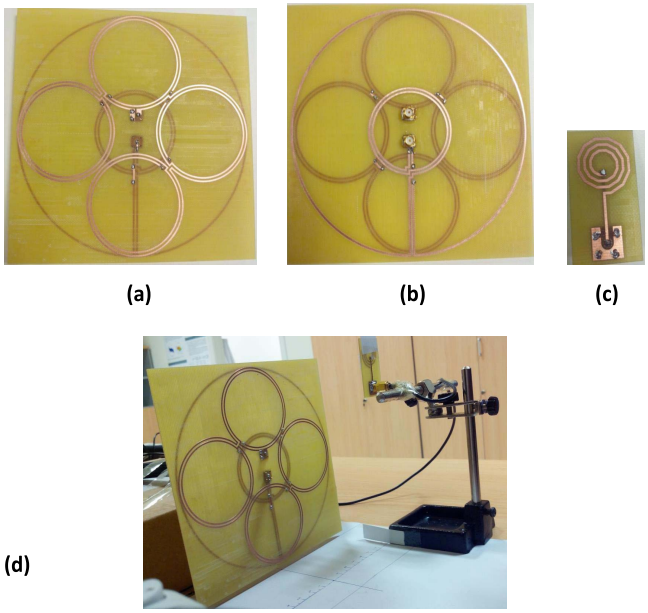

Fig. 11. Fabricated antennas. (a) Proposed design front. (b) Back. (c) Rx coil. (d) setup for measurement.

V. Antenna Fabrication and Measurements

In support to the analysis and the simulation of previous sections, we present fabrication and measurement of the proposed multicoil Tx antenna. The proposed antenna realized in Fig. 7 was fabricated and shown in Fig. 11(a) and (b). A small receiver (Rx) planar spiral coil antenna with outer diameter 1.9 cm was also fabricated as shown in Fig. 11(c) and used as near-field probe to measure H-field originating from the proposed Tx coil antenna. The input impedance of the Rx antenna was matched to 50 Ω at 13.56 MHz using L-section matching network consisting of two capacitors with values 421 pF and 110 pF, similar to the circuit shown in Fig. 7.

Using Agilent PNA-X Network Analyzer (connectors and cables appropriately calibrated, and fixture function used), the reflection coefficient (S11) of the antenna was measured and shown in Fig. 12. The near-field performance (H distribution) of the proposed Tx antenna was measured using small Rx coil and setup is shown in Fig. 11(d). The Tx antenna connected to port-1 of the network analyzer was fixed. The Rx coil connected to port-2 of the network analyzer was placed at a distance $z = 50$ mm away from the Tx antenna and moved to scan the x-axis and the y-axis to measure S21. During scanning process, a particular orientation of the Rx coil with

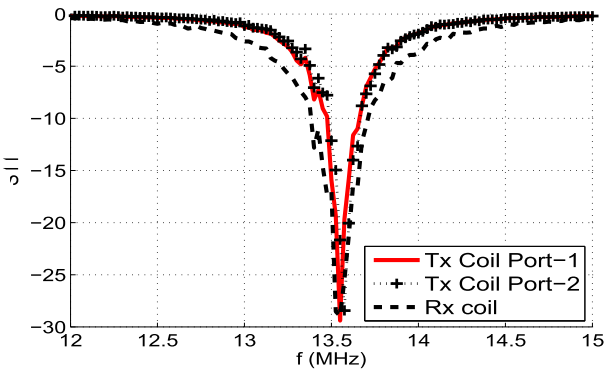

Fig. 12. Measured S11 response for the proposed coils.

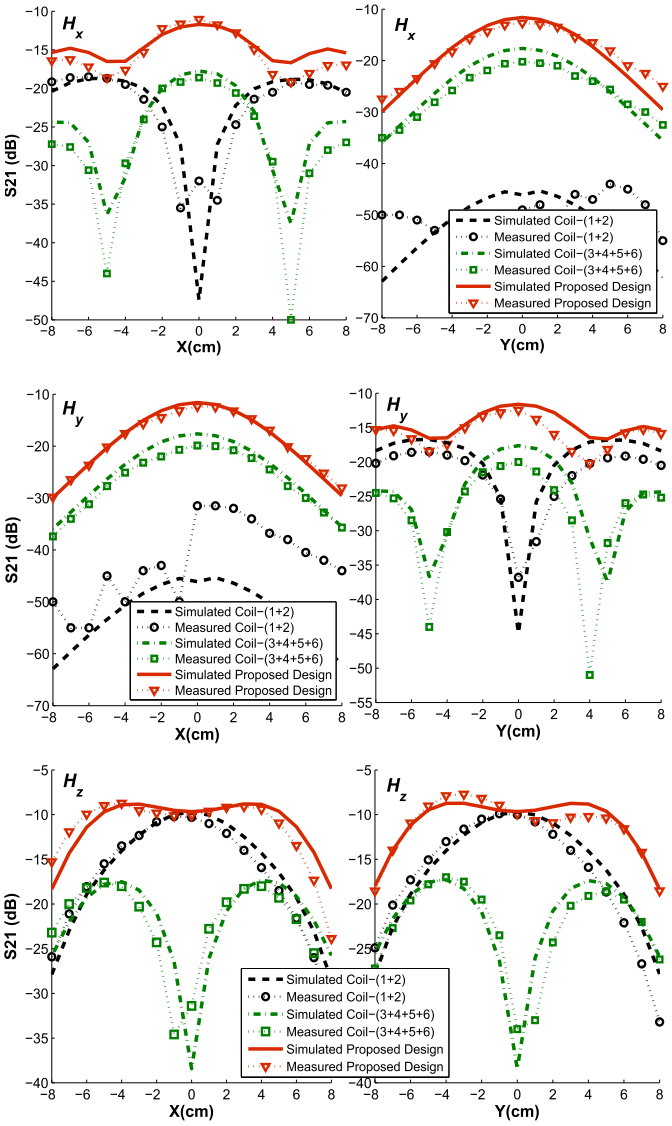

Fig. 13. Measured S21 results of the proposed coil antenna at $z = 50$ mm.

respect to the Tx coil indicates a particular component of H to be measured. For instance, the Rx coil perpendicular to z-axis (x-axis and y-axis) will result in H_z (H_x and H_y, respectively) measurement. The measured and simulated S21 representing H distributions are shown in Fig. 13.

The measured distributions of the components H_x, H_y, and H_z originating from coil-1-2, and coil-3-4-5-6, and the

proposed planar multicoil antenna is compared, considering the target Rx range $-2 \leq x \leq 2$, $-2 \leq y \leq 2$ in cm. For coil-1-2, the variations of H_x, H_y, and H_z measured and simulated in Fig. 13 are corroborating with analytical results of Fig. 2(a), showing that it contributes to H_z field forming in the target Rx area, whereas, H_x and H_y field components are vanishingly weak. However, for coil-3-4-5-6, the contribution of H_x and H_y field forming is apparent, whereas the H_z is weak, this corroborates with analysis shown in Fig. 3(a). Therefore, this justifies the contributions of coil-1-2 in H_z field forming and of coil-3-4-5-6 in H_x and H_y field forming. As apparent from the results of Fig. 13 for the proposed multicoil antenna, essentially, H_x, H_y, and H_z field forming is achieved validating the measurements and the results of Figs. 5 and 9. The analytical, simulated, and measured results corroborated the claims and proved the potential of the proposed planar multicoil antenna to be used as transmitter in inductive coupling systems for applications such as RFID, NFC, WPT, and medical implantation.

Though the proposed antenna produces three orthogonal H-fields, the in-phase components H_x and H_y, and the quadrature phase component H_z, this arrangement produces a resultant transverse field H_{xy} in xy-plane and a vertical field H_z having 90° phase difference. A planar Rx coil whose axis lies in xy-plane and perpendicular to H_{xy} vector is unable to capture any H-field. Hence there exists a direction in xy-plane in which the planar Rx coil could not have any induced voltage. This limitation is due to the fact that out of three field components (H_x, H_y, and H_z oscillating with same frequency) only one field component (H_z) may have 90° phase difference with other two field components (H_x, H_y) to maintain orthogonality in time. This motivates our future investigation to find solution of forming three H-field components, which are orthogonal both in direction and time to completely mitigate angular misalignment problem.

VI. Conclusion

In this paper, a planar multicoil antenna is proposed to be used in inductive coupling systems operating at 13.56 MHz and aimed to address angular misalignment problem by exploiting a magnetic field forming of three orthogonal H-field components in a target area. The antenna can therefore power planar receiving coils of almost all orientations in the surroundings. Initially, the H-field distributions of various combinations of spatially distributed coils were analyzed for the H-field forming in the near-field, which evolved into the proposed antenna consisting of six spatially distributed coils in a double-sided PCB for easy fabrication at low cost, where four coils contribute in forming lateral H-field components (H_x and H_y) and other two in forming axial H-field component (H_z), the orthogonality. The design was simulated and measured to validate the claims and results corroborated with the analysis. The design is considered as a good antenna candidate for wireless powering applications, e.g., RFID, medical implants, NFCs, and mobile consumables. Though the proposed antenna was designed for the applications where medium between the Tx and Rx coil has relative permeability $\mu_r = 1$ and the size of receivers are small enough, for other applications with magnetic medium the proposed magnetic field forming method is equally valid to generate the desired distribution of the orthogonal H-field components. However, the effects of proximity to the ground plane and the effects of mutual coupling on antenna detuning due to large Rx coil antennas need to be studied and intended to be compensated by adapting the matching networks of the Tx coil antenna, which is the future scope of the current design.

References

[1] Y. Lee. (2003). *Antenna Circuit Design for RFID Applications*. Microchip Technol. Inc. [Online]. Available: http://ww1.microchip.com/downloads/en/appnotes/00710c.pdf

[2] *Identification Cards—Contactless Integrated Circuit Cards—Proximity Cards—Part 3: Initialization and anticollision*, Standard ISO/IEC 14443-3, 2016. [Online]. Available: https://www.iso.org/standard/70171.html

[3] B. Jiang, J. R. Smith, M. Philipose, S. Roy, K. Sundara-Rajan, and A. V. Mamishev, "Energy scavenging for inductively coupled passive RFID systems," *IEEE Trans. Instrum. Meas.*, vol. 56, no. 1, pp. 118–125, Feb. 2007.

[4] K. Finkenzeller, *RFID Handbook*, 2nd ed. New York, NY, USA: Wiley, 2003.

[5] C. M. Zierhofer and E. S. Hochmair, "Geometric approach for coupling enhancement of magnetically coupled coils," *IEEE Trans. Biomed. Eng.*, vol. 43, no. 7, pp. 708–714, Jul. 1996.

[6] T. I. Inc. (Sep. 2003). *HF Antenna Design Notes*. [Online]. Available: http://www.ti.com/rfid/docs/manuals/appNotes/HFAntennaDesignNotes.pdf

[7] U.-M. Jow and M. Ghovanloo, "Design and optimization of printed spiral coils for efficient transcutaneous inductive power transmission," *IEEE Trans. Biomed. Circuits Syst.*, vol. 1, no. 3, pp. 193–202, Sep. 2007.

[8] W. Aerts, E. D. Mulder, B. Preneel, G. A. E. Vandenbosch, and I. Verbauwhede, "Dependence of RFID reader antenna design on read out distance," *IEEE Trans. Antennas Propag.*, vol. 56, no. 12, pp. 3829–3837, Dec. 2008.

[9] A. Sharma, I. J. G. Zuazola, A. Gupta, A. Perallos, and J. C. Batchelor, "Non-uniformly distributed-turns coil antenna for enhanced H-field in HF-RFID," *IEEE Trans. Antenna Propag.*, vol. 61, no. 10, pp. 4900–4907, Oct. 2013.

[10] J. Walk, J. Weber, C. Soell, R. Weigel, G. Fischer, and T. Ussmueller, "Remote powered medical implants for telemonitoring," *Proc. IEEE*, vol. 102, no. 11, pp. 1811–1832, Nov. 2014.

[11] E. G. Kilinc, M. A. Ghanad, F. Maloberti, and C. Dehollain, "A remotely powered implantable biomedical system with location detector," *IEEE Trans. Biomed. Circuits Syst.*, vol. 9, no. 1, pp. 113–123, Feb. 2015.

[12] C.-W. Chang, K.-C. Hou, L.-J. Shieh, S.-H. Hung, and J.-C. Chiou, "Wireless powering electronics and spiral coils for implant microsystem toward nanomedicine diagnosis and therapy in free-behavior animal," *Solid-State Electron.*, vol. 77, pp. 93–100, Nov. 2012.

[13] F. E. Hatmi *et al.*, "A multilayered coil antenna for ingestible capsule: Near-field magnetic induction link," *IEEE Antennas Wireless Propog. Lett.*, vol. 12, pp. 1118–1121, Jun. 2013.

[14] *WPC*. [Online]. Available: http://www.wirelesspowerconsortium.com

[15] E. G. Kilinc, G. Conus, C. Weber, B. Kawkabani, F. Maloberti, and C. Dehollain, "A system for wireless power transfer of micro-systems *in-vivo* implantable in freely moving animals," *IEEE Sensors J.*, vol. 14, no. 2, pp. 522–531, Feb. 2014.

[16] X. Liu and S. Y. R. Hui, "Optimal design of a hybrid winding structure for planar contactless battery charging platform," *IEEE Trans. Power Electron.*, vol. 23, no. 1, pp. 455–463, Jan. 2008.

[17] D. Zhao *et al.*, "Magnetic field forming of spatial multiple antennas for wireless power transfer," in *Proc. ISAP*, Nagoya, Japan, 2012, pp. 1204–1207.

[18] W. Chen, Z. Bai, S. Rickers, G. H. Bruck, and P. Jung, "Transmitter with cooperative coils matrix for robust wireless power transfer system," in *Proc. Int. Symp. Electromagn. Compat.*, Gothenburg, Sweden, Sep. 2014, pp. 48–52.

[19] S. A. Mirbozorgi, H. Bahrami, M. Sawan, and B. Gosselin, "A smart multicoil inductively coupled array for wireless power transmission," *IEEE Trans. Ind. Electron.*, vol. 61, no. 11, pp. 6061–6070, Nov. 2014.

[20] M. Q. Nguyen, Z. Hughes, P. Woods, Y.-S. Seo, S. Rao, and J.-C. Chiao, "Field distribution models of spiral coil for misalignment analysis in wireless power transfer systems," *IEEE Trans. Microw. Theory Techn.*, vol. 62, no. 4, pp. 920–930, Apr. 2014.
[21] R. Carta, J. Thoné, and R. Puers, "A wireless power supply system for robotic capsular endoscopes," *Sens. Actuators A, Phys.*, vol. 162, pp. 177–183, Jan. 2010.
[22] B. Lenaerts and R. Puers, "An inductive power link for a wireless endoscope," *Biosens. Bioelectron.*, vol. 22, pp. 1390–1395, Aug. 2007.
[23] T. Ishizaki, S. Nojiri, T. Ishida, and I. Awai, "3-D free-access WPT system for charging movable terminals," in *Proc. IMWS-IWPT*, 2012, pp. 219–222.
[24] Y. Lim and J. Park, "A novel phase-control-based energy beamforming techniques in nonradiative wireless power transfer," *IEEE Trans. Power Electron.*, vol. 30, no. 11, pp. 6274–6287, Nov. 2015.
[25] B. Lenaerts and R. Puers, "Inductive powering of a freely moving system," *Sens. Actuators A, Phys.*, vols. 123–124, pp. 522–530, Sep. 2005.
[26] W. Chen, S. Rickers, G. H. Bruck, and P. Jung, "Cooperative transmitter structure for improving efficiency in wireless power transfer," in *Proc. ISAP*, Kaohsiung, Taiwan, Dec. 2014, pp. 405–406.
[27] J. Kim, D. H. Kim, J. Choi, K. H. Kim, and Y. J. Park, "Free-positioning wireless charging system for small electronic devices using a bowl-shaped transmitting coil," *IEEE Trans. Microw. Theory Techn.*, vol. 63, no. 3, pp. 791–800, Mar. 2015.
[28] C. A. Balanis, *Antenna Theory Analysis and Design*, 2nd ed. Hoboken, NJ, USA: Wiley, 1997.

Ashwani Sharma received the B.Tech. degree from the LNM Institute of Informations Technology, Jaipur, India, in 2010, the M.Tech. degree in technology and communication systems from the Escuela Técnica Superior de Ingenieros de Telecomunicación de Madrid, Technical University of Madrid, Madrid, Spain, in 2013, and the Ph.D. degree from the University of Deusto, Bilbao, Spain, in 2015.

He was a Junior Research Fellow with IIT Delhi, New Delhi, India, from 2010 to 2011, a Visiting Training Fellow with the University of Kent, Canterbury, U.K., in 2014, and a Visiting Research Fellow with the Malaviya National Institute of Technology, Jaipur, India, in 2015. He has been an Assistant professor with the Jaypee University of Information Technology, Solan, India, since 2016. His research works have been published in various international journals and conferences such as IEEE TRANSACTIONS and Letters, *IET journals*, and *Wiley Letters*. His current research interests include near-field coil antennas, single and multiband antenna, and near-field forming.

Ghanshyam Singh (SM'16) received the B.E. degree from the National Institute of Technology, Silchar, India, in 1997, and the M.Tech. and Ph.D. degrees, all in electronics and communication engineering from Malaviya National Institute of Technology (MNIT), Jaipur, India, in 2003 and 2012, respectively.

He worked as a Visiting Researcher at HW University, Edinburgh, U.K., in 2009. He was a recipient of a CIMO Fellowship (by the Govt. of Finland) and worked at the University of Eastern Finland during January–June 2010, and was a Visiting Professor in the Department of EEE, Keio University, Japan, in October 2013. Presently, he is engaged in joint research projects with partner researchers from KEIO University, Tokyo, Japan, the University of, Vienna, Austria, Lviv Polytechnique Institute, Lviv Oblast, Ukraine, and the University of Cairo, Egypt. His current research interests include integrated photonics, antenna and RF engineering.

Dr. Singh became a Senior Member of OSA in 2016, is a Fellow of OSI and IETE, and is a Life member of other professional societies including the SPIE, ISTE, BESI, IE (India), etc. He was awarded "Distinguished Lecturer" by the IEEE Photonics Society for term 2017–18.

Deepak Bhatnagar (SM'00) received the M.Sc. and Ph.D. degrees in physics from the University of Rajasthan, Jaipur, India, in 1981 and 1986, respectively.

He is currently a Professor with the Department of Physics, University of Rajasthan, where he is the Director with the Center for Converging Technologies and has nearly 30 years of teaching and research experience. Eighteen students have obtained their Ph.D. degree under his supervision while he is currently leading a group of 8 researchers in the fields of microstrip antennas and components, dielectric relaxation properties nanomaterial, and conducting polymers. He has authored or co-authored over 150 papers in international and national journals and conference proceedings.

Dr. Bhatnagar is the fellow of the IETE (India) and a Life Member of several other societies.

Ignacio J. Garcia Zuazola (M'11–SM'15) received the FPII degree in industrial electronics from the School of Chemistry and Electronics, Indautxu, Spain, in 1995, the Higher National Diploma in telecommunications engineering from the University of Middlesex, London, U.K., in 2000, the B.Eng. degree in telecommunications engineering from Queen Mary University of London, in 2003, the Ph.D. degree (part-time program) in electronics (antennas) from the University of Kent, Canterbury, U.K., in 2010, and the e-MBA in Business (part-time program) with Cardiff Metropolitan University, Cardiff, U.K., in 2016.

He worked at Babcok and Wilcox, Bilbao, Spain in 1993, Iberdrola, Santurce, Spain, in 1995, Telefonica, Bilbao, in 1997, Thyssen Elevators, Bilbao, in 1998, and Cell Communications, Bilbao, in 2000, and engaged in an SME in electrical wiring at Gartzola, Bilbao, in 1996. He was formerly employed as a Research Associate with the University of Kent in 2004 and 2008, a Research Engineer (Grade 9/9) with the University of Wales, Swansea, U.K., in 2006, a Senior Research Fellow with the University of Deusto, Bilbao, in 2011, a Visiting Senior Research Fellow with the University of Leeds, Leeds, U.K., in 2011, and a Research Associate with Loughborough University, Loughborough, U.K., in 2014. He has been a Representative of Spain since 2015 with the London School of Commerce, U.K., and a Research Collaborator with the University of Deusto, Bizkaia, Spain, since 2015. His current research interests include business development on one hand and single-band and multiband miniature antennas, and the use of electromagnetic bandgap structures and frequency-selective surfaces.

Dr. Zuazola was a recipient of various awards in electrical wiring, pneumatic and hydraulic systems, and robotics.

Asier Perallos received the B.Sc., M.Sc., and Ph.D. degrees in computer engineering from the University of Deusto, Bizkaia, Spain.

He is an Associate Professor at the University of Deusto, where he is also the Dean of the Faculty of Engineering and a Principal Researcher of "Deusto Smart Mobility." He has more than 15 years of experience as a Lecturer with the Faculty of Engineering, University of Deusto, with a focus on software design and distributed systems. He has over a decade of experience in Research and Development Management, leading a number of projects and technology transfer actions. His current research interests include telematic systems, vehicular communication middleware, and intelligent transportation systems.